Morphological Segmentation of Textured Cell Images

Hai-Shan Wu, Joseph Barba,* and Joan Gil

Department of Pathology, Box 1194, Mount Sinai School of Medicine, 100th Street & 5th Avenue, New York, NY 10029
**Department of Electrical Engineering, City College of New York, 140th Street & Convent Avenue, New York, NY 10031*

An iterative morphological algorithm for segmentation of textured cell images encountered in cytology is introduced. The initial image segmentation is determined by classifying the image local variation information obtained with dilation and erosion operations. A median filter is then used to smooth the initially segmented image. A modified median filter is applied subsequently to correct possible classification errors inside the cells. The modified median filter can clear small regions of misclassified pixels while avoiding significant changes to the cell profiles. An erosion operation is finally used to restore the cell regions. Experimental results demonstrate that the proposed algorithm is successful. Comparison of the proposed algorithm and the K-means clustering method is provided.

Journal of Imaging Science and Technology 40:3 265–270 (1996)

Introduction

Segmentation of cell images is important in the application of computerized image analysis to medical pathology.[1] In pathology, automatic diagnoses of cancer, for instance, are based on subjective determinations of properties of cell nuclei by a trained pathologist.[2] Most of these properties (cell size, nuclear pleomorphism, nuclear irregularity, chromatin texture) can be objectively quantitated by the tools of image analysis. It is therefore possible to replace the subjective study of the cells of a tumor with a numerical description of their relevant properties. Hence, the diagnosis becomes a problem of pattern recognition.

The first step prior to study of the nuclear property is nuclear segmentation. This technique, when applied to cell nuclei, has a dismal record, which is attributable to the textured characteristics of both the nuclei and their background. Trained observers determine the location of the boundary by observation of a peripheral chromatin condensation, which amounts to a thickening of the nuclear measure. The importance of an accurate segmentation as the first step toward quantitation of the nuclear property is self-evident.[3]

Many algorithms are available for image segmentation. Edge-based segmentation methods are based on the idea of discontinuity of image intensities at the boundary between different objects.[4] Region-based algorithms employ region growing, region splitting, and merging to separate different objects with homogeneous intensities.[5,6] Unsupervised nonparametric clustering classifiers have also been extensively studied.[7,8] Most image segmentation methods assume that regions have relatively homogeneous intensities. However, natural biological cells may be textured and may have very complicated spatial contents. Currently, the most reliable segmentation methods are still interactive manual tracing and semiautomatic algorithms.[9] Although the segmentation of textured images has been studied extensively in the literature,[10–12] very little has been done for textured cells, which usually do not fit well-defined signal models. In this article, we introduce a segmentation algorithm for textured cell images based on morphological operations.

Algorithm

Let $f(n_1, n_2)$, for $(n_1, n_2) \in S$, represent the original image, where $S = \{(n_1, n_2) \mid n_1 = 0, 1, ..., N_1 - 1; n_2 = 0,1, ..., N_2 - 1\}$ and $N_1 \times N_2$ *is* the image size. Let the set $B_{(r)}$ be a circular region defined by $B_{(r)} = \{(n_1, n_2) | n_1^2 + n_2^2 \le r^2\}$. Considering the margin effects of the image, the dilation and erosion operations of image $f(n_1, n_2)$ by the structuring set $B_{(r)}$ are given by[13–15]

$$f_{\{e,B_{(r)}\}}(n_1,n_2) = \mathrm{dil}_{B_{(r)}}(f(n_1,n_2)) = \max_{\substack{(\xi_1+n_1,\xi_2+n_2)\in S \\ (\xi_1,\xi_2)\in B_{(r)}}} f(\xi_1+n_1,\xi_2+n_2), \quad (1)$$

and

$$f_{\{e,B_{(r)}\}}(n_1,n_2) = \mathrm{er}_{B_{(r)}}(f(n_1,n_2)) = \min_{\substack{(\xi_1+n_1,\xi_2+n_2)\in S \\ (\xi_1,\xi_2)\in B_{(r)}}} f(\xi_1+n_1,\xi_2+n_2), \quad (2)$$

for $(n_1, n_2) \in S$, respectively.

Initial Segmentation. For textured images, the difference between the variations of the cell and background intensities can be used as the pattern features to segment the cell regions from the background. The variation measure or morphological gradient[15] at location (n_1,n_2) is $v_{B_{(r)}}(n_1,n_2) = f_{\{d,B_{(r)}\}}(n_1,n_2) - f_{\{e,B_{(r)}\}}(n_1,n_2)$, for $(n_1,n_2) \in S$. If the morphological gradient $v_{B_{(r)}}(n_1,n_2)$is large, then the pixel at (n_1,n_2) will very likely belong to a cell region. In contrast, if the variation $v_{B_{(r)}}(n_1,n_2)$ is small, the pixel at (n_1,n_2) will probably be a background pixel. Thus a rough initial segmentation can be obtained by a simple thresholding procedure, such as:

$$t_{B_{(r)}}(n_1,n_2) = \begin{cases} 1, & \text{if } v_{B_{(r)}}(n_1,n_2) \ge T, \\ 0, & \text{otherwise,} \end{cases} \quad (3)$$

Original manuscript received July 19, 1995. Revised March 13, 1996.

for $(n_1,n_2)\in S$, where T is a constant. The binary image $t_{B_{(r)}}(n_1,n_2)$ uses value 1 to represent the initially segmented cell pixels and value 0 to represent the initially segmented background pixels. This initial segmentation may contain many classification errors, because the image signal is not ideally stationary and the large size of the $B_{(r)}$ region may reduce the resolution at the cell boundaries.

Elimination of Misclassified Regions Inside the Initially Segmented Cell Contours. Because the cell textures are not ideally stationary, many small misclassified regions usually occur within the cells. To correct these mistakes, a median filter with a large window seems appropriate. When a median filter with window $B_{(\rho)}$ is applied to the binary image $t_{B_{(r)}}(n_1,n_2)$, edges corresponding to large regions, such as the cell contours, will be smoothed and may contract a bit, depending on the size difference between the cell and $B_{(\rho)}$. All misclassified regions smaller than half the size of $B_{(\rho)}$ within the cell contours will be completely corrected. Larger misclassified regions within the cell contours will also shrink to varying degrees, depending on their sizes and shapes.

In general, all regions shrink, with smaller size regions shrinking more than larger size regions, and contours are smoothed. Repeated application of the median filter is expected to diminish the misclassified regions inside the cell. However, the median filter also shrinks the cell regions at the same time, and, although the shrinkage of the segmented cell region is not as great as that undergone by the small misclassified regions within the cell, the accumulation due to repeated application of the median filter is substantial.

To avoid the cumulative shrinkage of the cell region, the filter must be capable of eliminating the misclassified regions enclosed in the currently segmented cell region without altering the cell contours. The filter should be able to distinguish between misclassified cell pixels and correctly segmented noncell pixels. Incorporating the local neighborhood image information around a pixel will make it relatively easy to identify misclassified cell pixels that lie close to a cell region, as compared with misclassified pixels that are located far from any cell region. If application of the filter can correct some of the misclassified cell pixels near the cell regions, then repeated applications of the filter may shrink the misclassified regions progressively.

Figure 1 shows four typical examples of the local neighborhood around the center pixel, indicated by thick block lines, which is currently being identified in a segmented image. The ones and zeros denote cell and noncell pixels, respectively. Because the center values of Fig. 1(b) and 1(c) are 1, representing cell pixels, their status should not be altered. In Fig. 1(a), there are more zeros than ones and the edge curve surrounds the cell region; thus the center pixel is most likely a noncell pixel next to a cell region and should not be altered. In Fig 1(d), however, there are more ones than zeros and the edge curve surrounds the zeros region; thus the center pixel is most likely a misclassified pixel inside the cell region and should be changed to a cell pixel.

To implement such operations, we define the modified median filtering of the image $t_{B_{(\rho)}}(n_1,n_2)$, by the set $B_{(\rho)}$ as:

$$t_{\{mm,B_{(\rho)}\}}(n_1,n_2)=\begin{cases}1, & \text{if } M_{\{1,t_{B_{(r)},B_{(\rho)}\}}}(n_1,n_2)\geq M_{\{0,t_{B_{(r)},B_{(\rho)}\}}}(n_1,n_2),\\ t_{B_{(r)}}(n_1,n_2) & \text{otherwise,}\end{cases}\tag{4}$$

for $(n_1,n_2)\in S$. The high-order modified median filtering of the binary image $t(n_1,n_2)$ with the set $B_{(\rho)}$ *is* defined recursively by:

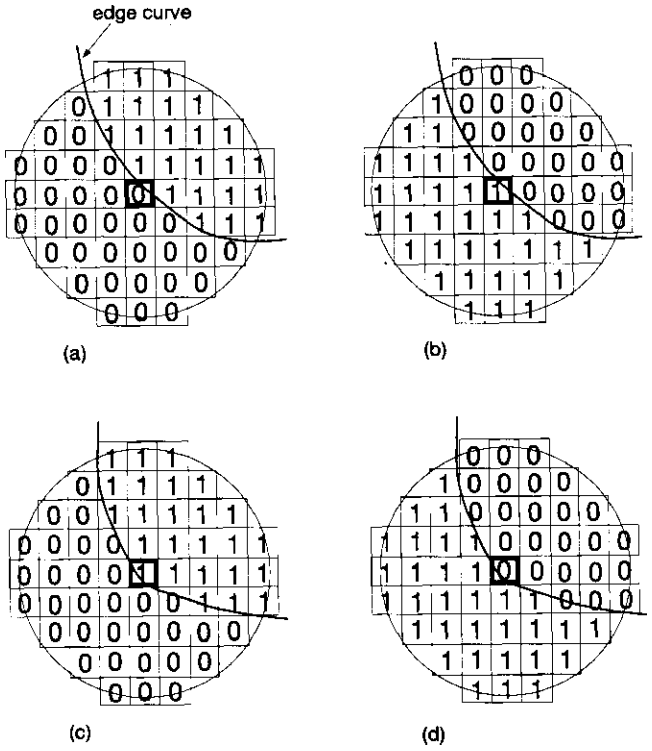

Figure 1. Typical segmentation samples of local images within a circular window, where the values 1 and 0 denote the previously classified cell and noncell pixels, respectively, and the center pixel is marked. Because the filter does not shrink cell regions, the center values of (b) and (c) should not be altered. In (a), there are more zeros than ones and the edge curve is likely to surround the cell region; thus the center pixel should not be altered. In (d), there are more ones than zeros and the edge curve surrounds the previously segmented non-cell region; thus the center pixel should be altered from 0 to 1.

$$t^{(k)}_{\{mm,B_{(\rho)}\}}(n_1,n_2)=\begin{cases}1, & \text{if } M_{\{1,t^{(k-1)}_{\{mm,B_{(\rho)}\}},B_{(\rho)}\}}(n_1,n_2)\geq M_{\{0,t^{(k-1)}_{\{mm,B_{(\rho)}\}},B_{(\rho)}\}}(n_1,n_2)\\ t^{(k-1)}_{(mm,B(\rho)}(n_1,n_2) & \text{otherwise,}\end{cases}\tag{5}$$

for $(n_1,n_2)\in S$ and $k\geq 1$, where $t^{(0)}_{\{mm,B_{(\rho)}\}}(n_1,n_2)=t(n_1,n_2)$.

In modified median filtering, if a cell pixel is believed to be misclassified, it is changed to a cell pixel; otherwise, it remains unaltered. Thus, the modified median filter avoids changing cell pixels on cell contours to background pixels and continues to shrink previously misclassified holes within the cell. Although a small percentage of pixels are supposed to be corrected when using the filter once, large misclassified holes inside cell regions can eventually be eliminated by repeatedly applying the same filter. The iterative procedure must converge, because in each iteration the alteration of pixel values proceeds in only one way, from zero to one.

Restoration of Cell Contours. The above extracted contours are usually larger than the true cell contours because of the dilation and erosion operation in which the structuring set $B_{(r)}$ is used to obtain the variation image. Thus, the segmented cell regions represent the actual cell regions dilated by the structuring set $B_{(r)}$. To approximate the actual cell regions, the inverse operation, erosion, must be performed with the same structuring set $B_{(r)}$. Thus, the final segmented image becomes:

$$\mathrm{seg}(n_1,n_2) = \min_{\substack{(\xi_1+n_1,\xi_2+n_2)\in S \\ (\xi_1,\xi_2)\in B_{(r)}}} t^{(k)}_{\{mm,B_{(\rho)}\}}(\xi_1+n_1,\xi_2+n_2), \quad (6)$$

for $(n_1,n_2)\in S$. The cell contours can then easily be obtained based on the segmented image $\mathrm{seg}(n_1,n_2)$ by:[15]

$$c(n_1,n_2) = |\mathrm{seg}(n_1,n_2) - \max_{\substack{(\xi_1+n_1,\xi_2+n_2)\in S \\ (\xi_1,\xi_2)\in B_{(1.5)}}} \mathrm{seg}(\xi_1+n_1,\xi_2+n_2)|. \quad (7)$$

The image $c(n_1,n_2)$ is binary with values 1 and 0 representing contour and noncontour pixels, respectively.

The Segmentation Procedure. If the original cell image is somewhat noisy, a low-pass filter is required as a preprocessing step to reduce image noise so that the subsequent procedure is less sensitive to the image noise. The subsequent segmentation procedure is summarized as follows:

Step 0: Given a cell image represented by the two-dimensional function $f(n_1,n_2)$, for $(n_1,n_2)\in S$, specify the circular regions $B_{(r)}$ and $B_{(\rho)}$ with radii r and ρ, respectively. Set the threshold T.

Step 1: Compute the variation function $v_{B_{(r)}}(n_1,n_2)$, for $(n_1,n_2)\in S$. The initial segmentation $t_{B_{(r)}}(n_1,n_2)$, for $(n_1,n_2)\in S$, is obtained from Eq. 3. Apply the median filter with the structuring set $B_{(\rho)}$ to the binary image $t_{B_{(r)}}$ and obtain the processed image $t_{\{m,B_{(\rho)}\}}$. Let $t^0_{\{mm,B_{(\rho)}\}} = t_{m,B_{(\rho)}}$ and $k = 1$.

Step 2: Compute $t^k_{\{mm,B_{(\rho)}\}}$, the modified median filtering of the image $t^{k-1}_{\{mm,B_{(\rho)}\}}$ from Eq. 5.

Step 3: Measure the difference between the modified median filtered image, $t^k_{\{mm,B_{(\rho)}\}}$, and its input image, $t^{k-1}_{\{mm,B_{(\rho)}\}}$, by:

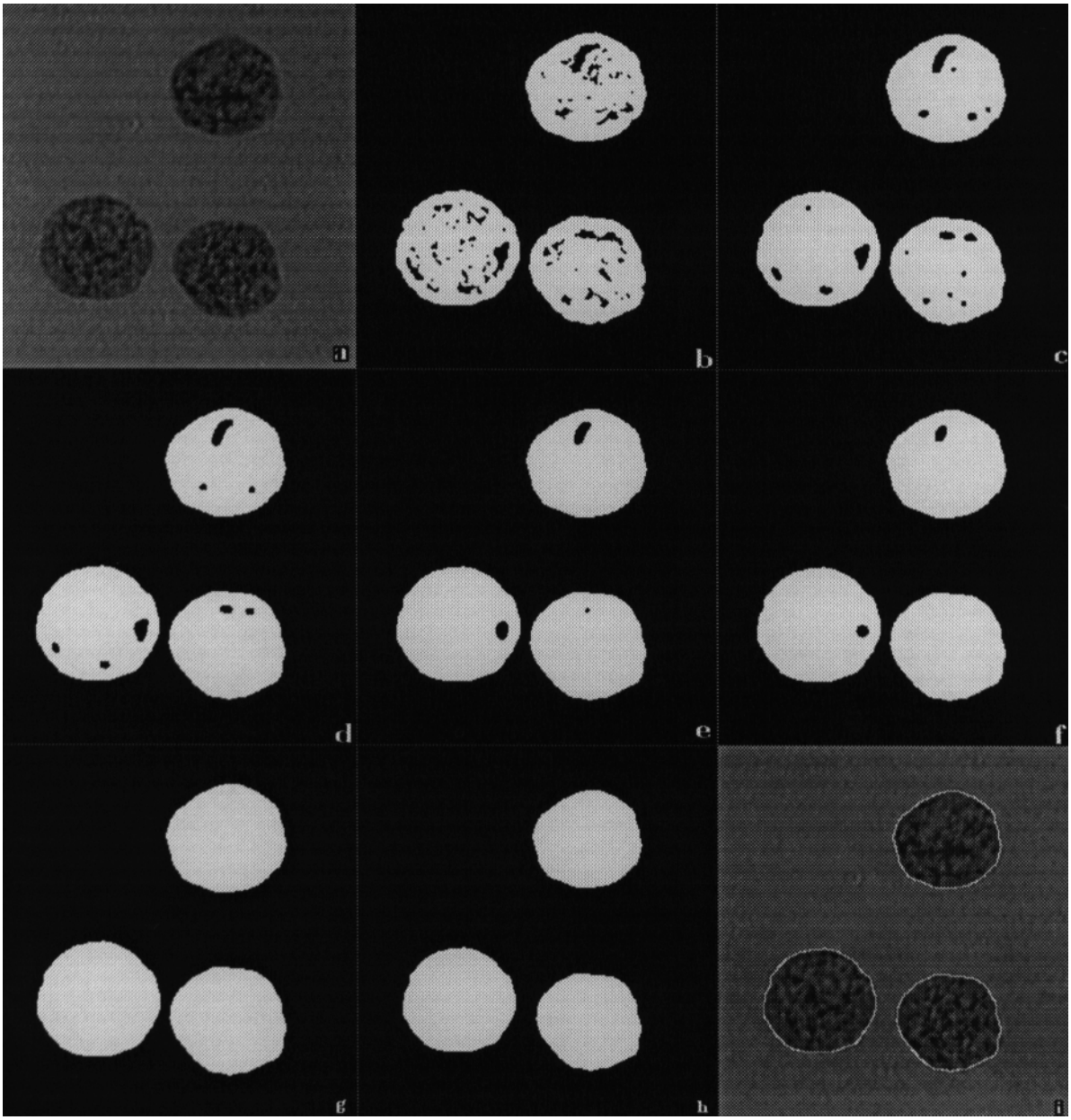

Figure 2. Evolution of the proposed segmentation algorithm for a cell image. (a) Original cell image of size 274×260, magnification 100×; (b) initial segmentation of the variation image obtained by morphological dilation and erosion operations with structuring set $B_{(4)}$; (c) median filtering of the image in (b) with the window $B_{(3.5)}$. Results of modified median filtering of the image in (c) with the window $B_{(3.5)}$: (d) 1, (e) 4, (f) 9, and (g) 16 times. (h) Final image segmentation obtained by eroding the images in (g) with the structuring set $B_{(4)}$. (i) The cell image with the extracted cell contours superimposed to show the performance of the segmentation visually.

$$\epsilon = \sum_{n_1=0}^{N_1-1}\sum_{n_2=0}^{N_2-1}(t^k_{\{mm,B(\rho)\}}(n_1,n_2) - t^{k-1}_{\{mm,B(\rho)\}}(n_1,n_2))^2. \quad (8)$$

If ϵ is not 0, go back to Step 2 for the next iteration; otherwise, execute Step 4.

Step 4: The final segmented image is obtained by an erosion operation on the binary image $t^k_{\{mm,B(\rho)\}}$, with the structuring set $B_{(r)}$ as:

$$\mathrm{seg}(n_1,n_2) = \min_{\substack{(\xi_1+n_1,\xi_2+n_2)\in S \\ (\xi_1,\xi_2)\in B_{(r)}}} t^k_{\{mm,B_{(\rho)}\}}(\xi_1+n_1,\xi_2+n_2), \quad (9)$$

for $(n_1,n_2)\in S$.

Experimental Results

In this section we provide the results for segmenting real textured cell images, using the proposed segmentation algorithm. Figure 2(a) and Fig. 3(a) are two original cell images of size 274 × 260 and 240 × 211, respectively. The cells are highly textured with large gray-level variations compared with the rather homogeneous background. To segment these textured cell images, the local gray-level variations are used as the classification feature where the variations are defined as the difference between the dilated and eroded original images. Because morphological dilation and erosion are sensitive to image noise, a preprocessing filtering procedure is used to reduce the image noise and make the segmentation algorithm more robust. In our experiments we used a linear shift invariant low-pass filter with cylinder spatial impulse response. The filtering process is implemented by:

$$f_o(n_1,n_2) = \frac{1}{M_\lambda(n_1,n_2)} \underbrace{\sum_{\xi_1=0}^{N_1-1}\sum_{\xi_2=0}^{N_2-1}}_{\substack{(\xi_1+n_1,\xi_2+n_2)\in S \\ (\xi_1,\xi_2)\in B_{(\lambda)}}} f_i(\xi_1+n_1,\xi_2+n_2), \quad (10)$$

where $B_{(\lambda)} = \{(\xi_1,\xi_2)|\xi_1^2+\xi_2^2 \le \lambda^2\}$, and $M_\lambda(n_1,n_2)$ is the number of elements in the set $\{(\xi_1,\xi_2)|\xi_1^2+\xi_2^2 \le \lambda^2\}$, & $(\xi_1+n_1,\xi_2+n_2)\in S$. The number of elements $M_\lambda(n_1,n_2)$ is constant except for regions near the boundary of the image support, where it depends on the position (n_1,n_2).

The simulations shown in Figs. 2 and 3 use identical preprocessing low-pass filters with $\lambda = 3$. The dilation and erosion operations with $r = 4$ are performed on the filtered images to obtain the variation images. This is followed by a simple thresholding procedure to convert each gray-level variation image into a binary image representing the initial rough segmentation. Figure 2(b) and Fig. 3(b) show the two initial segmented images of the filtered images in Fig. 2(a) and Fig. 3(a), respectively, where the threshold T is specified to be 20 in both simulations. It is observed that the initial segmentation is rather rough and contains numerous small misclassified regions, particularly within the segmented cells.

Figure 2(c) and Fig. 3(c) are the median filtering results of the initial segmented images in Fig. 2(b) and Fig. 3(b), respectively, using the same window $B_{(\rho)}$, with $\rho = 3.5$. Comparing Fig. 2(c) and Fig. 3(c) with Fig. 2(b) and Fig. 3(b), respectively, we observe that all misclassified regions shrink, with small misclassified regions being eliminated, and the segmented cell boundary becomes smoother. Figure 2(d)–(g) are the resulting images after applying the modified median filter to the image in Fig. 2(c) 1, 4, 9, and 16 times, respectively, with the same window $B_{(3.5)}$. Figures 3(d)–(g) are the resulting images after applying the modified median filter to the image in Fig. 3(c) 1, 2, 3, and 4 times, respectively, with the same window $B_{(3.5)}$. Figure 2(h) and Fig. 3(h) are the final respective segmentations of the two original images obtained by eroding the images of Fig. 2(g) and Fig. 3(g), respectively, with the same structuring sets $B_{(4)}$. To evaluate the segmentation visually, the extracted cell contours in Fig. 2(h) and Fig. 3(h) are displayed in Fig. 2(i) and Fig. 3(i) superimposed on the original images. Observe that the extracted contours match the cell profiles.

To measure the quantitative performance of the proposed algorithm, the cell images are segmented by careful manual tracing. The tracing results, which are assumed to be the correct segmentation, are shown in Fig. 4(a) and Fig. 5(a), respectively. Comparing the segmentations of Fig. 2(h) and Fig. 3(h) with the respective Fig. 4(a) and Fig. 5(a), the numbers of misclassified pixels are 0.9138% and 1.2046%. Figure 4(b) and 5(b) are the respective segmentation results of the two cell images in Fig. 2(a) and Fig. 3(a), using the K-means clustering algorithm.[7,8] Compared with the misclassification rates, 0.9138% and 1.2046%, of the proposed algorithm, the misclassification rates of the K-means clustering method are 2.8706% and 3.6868%, respectively.

It is known that the morphological closing operations can be used for hole filling. For comparison, the results of the closing operations on the initially segmented image in Fig. 2(b) with structuring sets $B_{(r)}$ of variant r are displayed in Fig. 6. Figure 6(a) shows the output of the closing operator with $B_{(3)}$. It is observed that the resulting image contains misclassified pixels within the cells. When the radius of the structuring set is increased to 5, as shown in Fig. 6(c), all holes are filled out, but the two closely located isolated cells are connected. Figure 6(b) shows a result intermediate between Figs. 6(a) and 6(c), wherein the radius of the structuring set is 4. The resulting segmentation has errors, and the two isolated cells are touching. Because the modified median filter does not dilate the cell regions, the isolated cell regions always remain disconnected, as seen in Fig. 2.

Summary and Conclusions

This article describes a segmentation algorithm for textured cell images, using morphological operations. A linear shift invariant low-pass preprocessing filter is applied to suppress image noise. The image variation function is related to the image local information and is obtained via dilation and erosion operations. The variation function undergoes a thresholding procedure to obtain a rough initial segmentation. The initial segmentation is improved by applying median filtering, followed by repeated applications of the modified median filter, and finally by an erosion filter. The modified median filter is applied once to smooth the current cell contours and shrink the misclassification regions inside the contours. The modified median filter is applied repeatedly until no further changes occur. This process completely corrects the misclassified regions within the segmented cell contours to obtain the solid cell regions. Finally, erosion with the same structuring set as that used in computing the variation function is applied to the binary image to obtain the final segmentation of the cell image. The superimposed images show that the extracted cell contours fit the real cell contours very well and therefore that the algorithm is successful in segmenting textured cell images. Quantitative evaluation is provided and compared with that of the nonparametric clustering classification method.

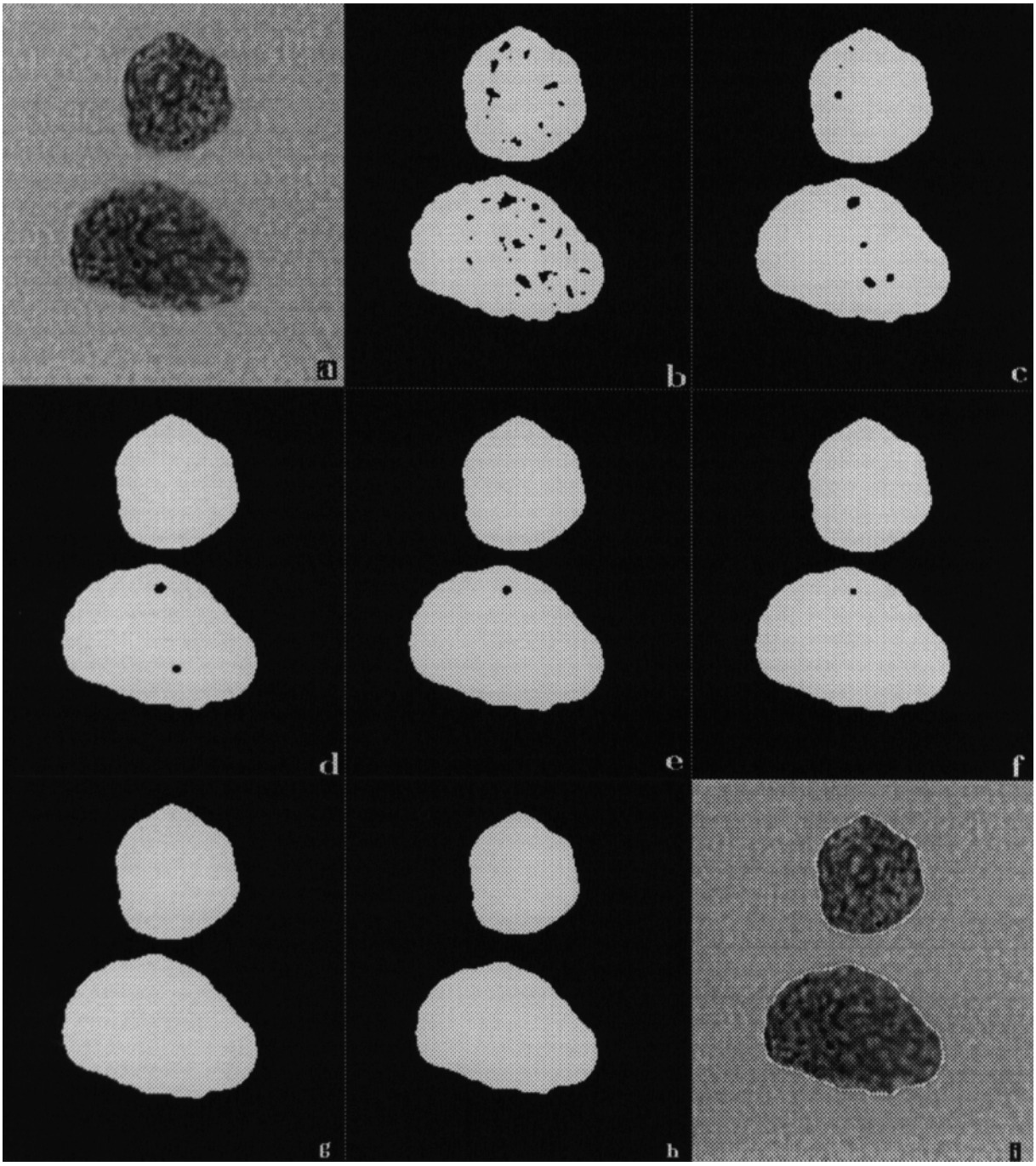

Figure 3. Evolution of the proposed algorithm for segmentation of another cell image. (a) Original cell image of size 240 × 211, magnification 100×; (b) initial segmentation based on classifying the variation classification features obtained by morphological dilation and erosion operations with the structuring set $B_{(4)}$; (c) median filtering of the image in (b) with the window $B_{(3.5)}$. Results of modified median filtering of the image in (c) with the window $B_{(3.5)}$: (d) once, (e) twice, (f) three times, and (g) four times. (h) The final segmentation obtained by eroding the images in (g) with the structuring set $B_{(4)}$. (i) The cell image with the extracted cell contours superimposed to show the performance of the segmentation visually.

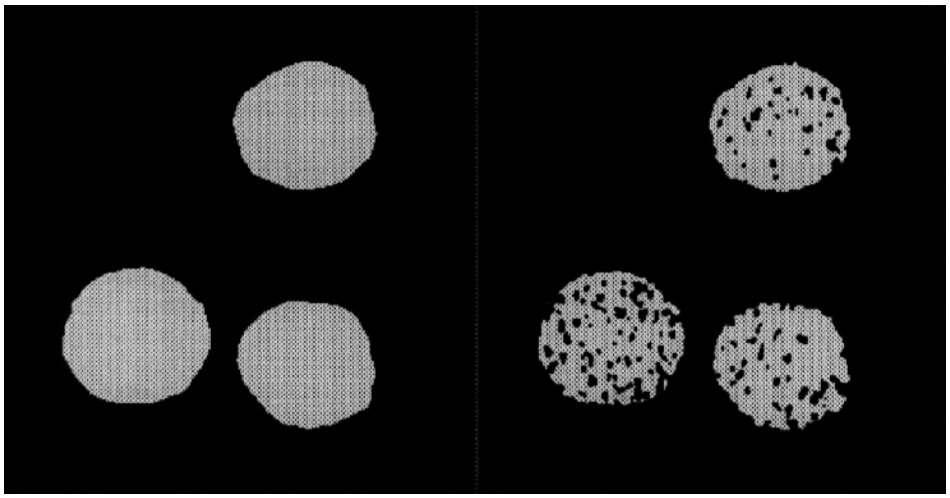

(a) (b)

Figure 4. Results of (a) manual tracing and (b) K-means clustering segmentation methods for the cell image shown in Fig. 2(a).

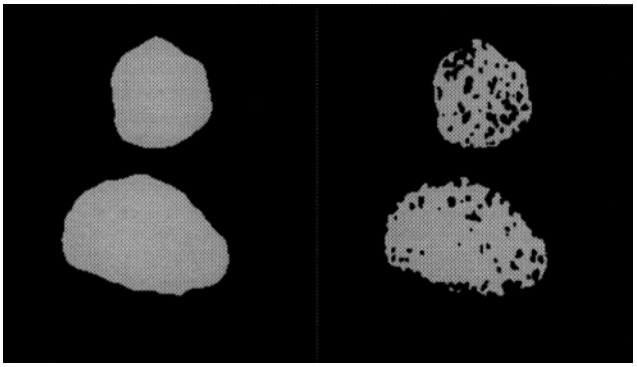

(a) (b)

Figure 5. Results of (a) manual tracing and (b) K-means clustering segmentation methods for the cell image shown in Fig. 3(a).

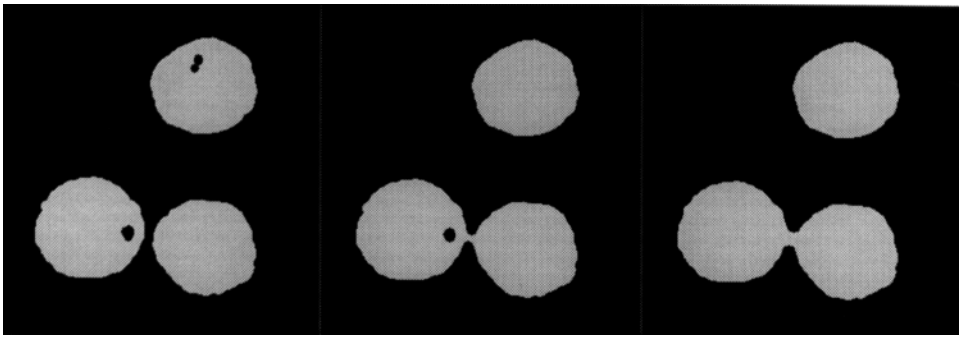

(a) (b) (c)

Figure 6. Morphological closing operations on the initially segmented image in Fig. 2(b) by circular structuring sets with radius sizes of (a) 3, (b) 4, and (c) 5.

Acknowledgment. This research was supported in part by the National Science Foundation, Grant CDA-9114481.

References

1. A. M. Marchevsky, J. Gil, and H. Jeanty, Computerized interactive morphometry in pathology: current instrumentation and methods, *Human Pathol.* **18**: 320–331 (1987).
2. A. J. Einstein, J. Barba, P. D. Unger, and J. Gil, Nuclear diffuseness as a measure of texture: Definition and application to the computer-assisted diagnosis of parathyroid adenoma and carcinoma, *J. Microscopy* **176**: l58–166 (1994).
3. J. Gil and J. Barba, Principles of stereology: Computerized applications to anatomic pathology, in *Image Analysis: A Primer for Pathologists,* A. M. Marchevsky and P. H. Bartels, Eds., Raven Press, New York, 1994, pp. 79–124.
4. J. Canny, Computational approach to edge detection, *IEEE Trans. Pattern Anal. Machine Intell.,* **8**: 679–698 (1986).
5. X. Wu, Adaptive split-and-merge segmentation based on piecewise least-square approximation, *IEEE Trans. Pattern Anal. Machine Intell.* **15**: 808–815 (1993).
6. H.-S.Wu, and J. Barba, An algorithm for noisy cell contour extraction via area merging, *J. Imaging Sci. Technol.* **38**: 604–607 (1994).
7. R. P. Lippmann, Pattern classification using neural networks, *IEEE Commun. Magazine,* 47–64 (1989).
8. C. Garbay, Image structure representation and processing: A discussion of some segmentation methods in cytology, *IEEE Trans. Pattern Analysis, Machine Intell.,* **8**: l40–146 (1986).
9. H.-S.Wu and J. Barba, An efficient semi-automatic algorithm for cell contour extraction, *J. Microscopy* **179**: 270–276 (1995).
10. A. Laine and J. Fan, Texture classification by wavelet packet signatures, *IEEE Trans. Pattern Anal. Machine Intell.,* **15**: 1186–1191 (1993).
11. H. Derin and H. Elliott, Modeling and segmentation of noisy and textured images using Gibbs random fields, *IEEE Trans. Pattern Anal. Machine Intell.* **9***:* 39–55 (1987).
12. Z. Fan and F. Cohen, Textured image segmentation as a multiple hypothesis test, *IEEE Trans. Circuits Syst.* **35**: 691–702 (1988).
13. H. J. A. M. Heijmans, *Morphological Image Operators*, Academic Press, New York, 1994.
14. E. R. Dougherty, Ed., *Mathematical Morphology in Image Processing*, Marcel Dekker, New York, 1993.
15. J. Serra, *Image Analysis and Mathematical Morphology*, Academic Press, New York, 1982.